ELSEVIER

Nuclear Instruments and Methods in Physics Research A 478 (2002) 527–537

NUCLEAR INSTRUMENTS & METHODS IN PHYSICS RESEARCH Section A

www.elsevier.com/locate/nima

Investigation of charge sharing among electrode strips for a CdZnTe detector

E. Kalemci*, J.L. Matteson

Center for Astrophysics and Space Sciences, 0424, University of California, San Diego, 9500 Gilman Dr., La Jolla, CA 92093-0424, USA

Received 6 July 2000; received in revised form 14 December 2000; accepted 24 February 2001

Abstract

We have investigated charge sharing among the anode strips of a CdZnTe (CZT) detector using a 30 μm collimated gamma-ray beam. We compared the laboratory measurements with the predictions from our modeling of the charge transport within the detector. The results indicate that charge sharing is a function of the interaction depth and the energy of the incoming photon. Also, depending on depth, a fraction of the electrons might drift to the inter-anode region causing incomplete charge collection. Here, we show that photoelectron range and diffusion of the charge cloud are the principal causes of charge sharing and obtain limits on the size of the electron cloud as a function of position in the detector.

PACS: 29.40.W; 07.85.F; 66.30

Keywords: CdZnTe; CZT detectors; Strip detectors; Solid-state detectors; X-ray astronomy

1. Introduction

CZT has desirable features for detection of high energy X-rays and low energy gamma-rays. Due to its high atomic number, $Z \sim 50$, photoelectric interactions dominate up to 250 keV. Its large bandgap (~ 1.54 eV) and high bulk resistivity ($\sim 10^{11}\,\Omega$ cm) result in low leakage current and noise [1], making it possible to achieve good energy resolution at room temperature. Its energy response is linear over the energy range of five to several hundred keV [2]. However, with a conventional planar configuration, a low energy tail appears due to incomplete hole collection in the pulse height spectrum of a monoenergetic source. Strip or pixel detectors can eliminate this problem by virtue of the small pixel effect [3,4].

We have developed and tested position-sensitive cross-strip CZT detectors for use in X-ray astronomy in collaboration with Washington University in St. Louis [1,2,5]. Previously, we modeled charge drift in the detectors and charge induction on the electrodes as a function of time to obtain a better understanding of these detectors. The model agreed very well with the measurements of total charge. The details of this modeling can be found in Kalemci et al. [1].

The motivations behind the present study were to test the part of the simulation dealing with the charge drift trajectories and to understand how charge sharing among the anodes affects the

*Corresponding author. Tel.: +1-858-534-6431.

E-mail address: emrahk@mamacass.ucsd.edu (E. Kalemci).

0168-9002/02/$ - see front matter
PII: S0168-9002(01)00892-0

performance of our detector. In this paper, the term "charge sharing" means that the electrons created by some interactions are collected by more than one anode strip. We attribute charge sharing to photoelectron range and diffusion of the resulting electron cloud. Depending on the distance between electrodes and the potential distribution in the detector, some of the electrons in this cloud might drift to inter-anode regions and cause incomplete charge collection, thereby distorting spectra and reducing energy resolution. Moreover, the size of the charge sharing region may limit the achievable spatial resolution. In our study, we measured the size of the diffusion cloud and its dependence on depth of interaction.

Our experimental approach was to use a collimated gamma-ray beam to scan across the electrodes of a cross-strip CZT detector and to analyze the observed pulse heights. Similar studies have been done by other groups with pixel detectors. Du et al. [6] and He et al. [7] investigated charge sharing in 3-D position sensitive CdZnTe spectrometers and obtained sizes of electron clouds for different gamma-ray sources. Bolotnikov et al. [8] studied the charge loss to inter-pixel gaps. Prettyman et al. [9] examined the charge sharing effect on coplanar grid detectors and investigated the gap events.

2. CZT strip detector

For our measurements, we used the UCSD-WU laboratory prototype detector (see Fig. 1) which was developed to study techniques for X-ray imaging applicable to astronomical instruments such as HEXIS [5] and MARGIE [10]. This $12 \times 12 \times 2\ \mathrm{mm}^3$ detector is configured with 22 anode strips on one side and 22 cathode strips on the other side. The cathode strips are orthogonal to the anode strips creating, in effect, a grid of 500 μm pixels. To enhance charge collection on the anodes, a set of steering electrodes is interlaced with the anodes. These steering electrodes are all connected to each other (see Fig. 2). Anodes and steering electrodes are 100 μm wide, while cathodes are 450 μm wide. The pitch size is 500 μm. The anodes are biased at 200 V and the steering electrode at 180 V, causing most electrons drifting towards the anode side of the detector to be directed away from the inter-anode region and towards an anode. A ceramic carrier holds the detector, that is always illuminated from the cathode side to minimize signal loss due to hole trapping. It was manufactured from "discriminator grade" material by eV Products.

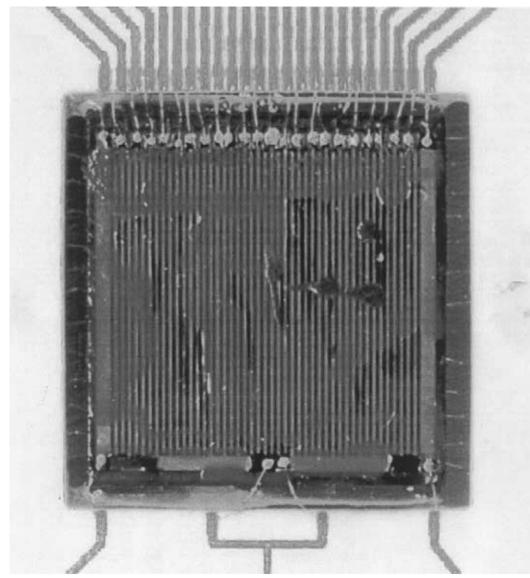

Fig. 1. Prototype CZT strip detector. The anode side is shown, with its 22 anode strips with 500 μm pitch and 22 interlaced steering electrodes. Total size is $12 \times 12 \times 2\ \mathrm{mm}^3$.

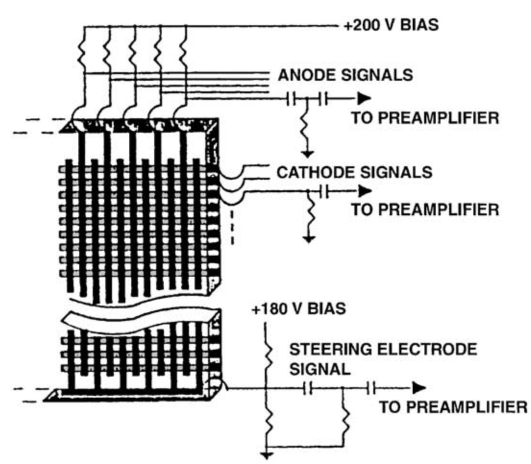

Fig. 2. Detector electrode and bias network connections.

3. Charge collection model

We developed a computer simulation of solid state detectors that predicts induced charge on each electrode for various electrode geometries and various interaction positions. We first calculate the electric fields and weighting potentials by using a general purpose program Maxwell 2D Field Simulator [12]. We specify the appropriate geometry, electrode pattern and potentials. We use a dielectric constant of 10. The Maxwell software iteratively calculates the electrostatic field solution by finite element analysis. Fig. 3 shows the result of the Maxwell electric field calculation for the UCSD-WU strip detector described in Section 2. We then transport the charges using the electric fields, electron and hole mobilities and trapping times and calculate the induced charge on each electrode using Ramo's weighting potential method [11]. The simulation takes charge trapping into account, but the effects of space charge and detrapping are not included. (Further information on the model is presented by Kalemci et al. [1].)

Our previous "non-diffusive" work modeled the ideal case where each interaction occurred at a point, with no lateral extension of the charge cloud. In this case the electrons and holes follow a single electric field line. Depending on the interaction position there are three cases. With reference to Fig. 3, electrons can follow: (1) solid lines (89% of the detector volume) and be collected by the anodes, (2) dashed lines (8%) and be collected by the steering electrode, or, (3) dotted lines (3%) and drift to the gap, in which case the signal is shared between an anode and the steering electrode.

In Kalemci et al. [1] we discussed each case and showed experimental evidence that electric field lines end at the steering electrode and the gaps as predicted by the simulation. Electrons reaching these positions will yield reduced anode signal, hence a low energy tail in the spectrum.

However, this previous simulation did not include important additional effects which broaden the distribution of charges. These are described in the next section. By including these effects, we have obtained a more accurate model of our detector.

4. Size of the electron cloud

When the incident X-ray interacts with the detector material, a photoelectron is ejected. This photoelectron loses energy by ionization, creating electron–hole pairs along its path until it is stopped. Therefore, X-ray interactions produce electron and hole distributions that are elongated along the path of the photoelectron. We call these distributions "clouds". The range of the photoelectron depends on the energy of the interaction.

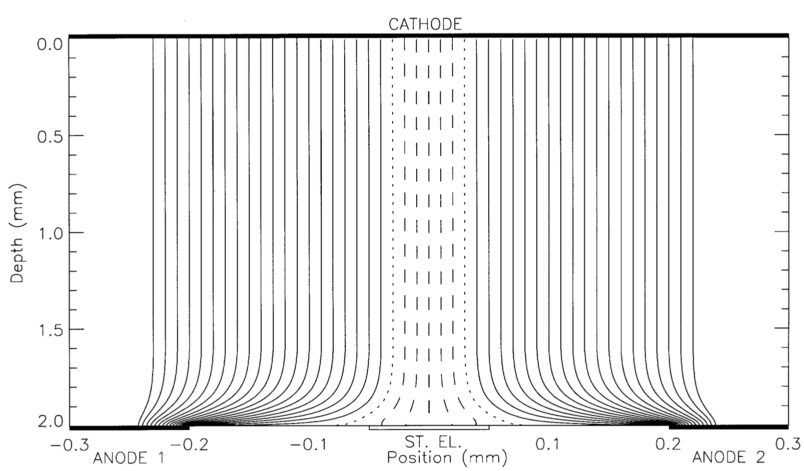

Fig. 3. Model calculation of electric field lines. Position and depth axes have different scales. Field lines terminate at the anodes (solid lines), steering electrodes (dashed lines), or in the inter-electrode gaps (dotted lines).

For example, a 40 keV photoelectron is stopped in 10 μm, whereas a 100 keV photoelectron is stopped in 47 μm [13]. These clouds are not uniform in charge density, since electron–hole production increases towards the end of the track. For a 100 keV photoelectron, 30% of the electron–hole pairs are created in the last 7 μm of its track. A K X-ray of $\sim$25 keV may also be produced in the initial interaction with mean free path of $\sim$85 μm, and its charge cloud will add to the overall distribution of charge in the detector.

Moreover, the clouds diffuse while drifting to the electrodes, making them larger. The diffusion of a material with concentration M is characterized by Fick's equation [14]:

$$D\nabla^2 M = \frac{\partial M}{\partial t} \tag{1}$$

where D is the diffusivity (or Einstein coefficient). D can be obtained from the Einstein relation, $D = \mu kT/e$, and it is $\sim 26\ \mathrm{cm}^2/\mathrm{s}$ for electrons at room temperature with mobility, μ, of $1000\ \mathrm{cm}^2/\mathrm{V\,s}$. For electrons, the travel time of $\sim$0.2 μs for a 2 mm thick detector is much shorter than the trapping time, $\sim$3 μs; therefore, we must use the time-dependent solution. The one dimensional solution for concentration $M(x,t)$ at position x and time t for a delta function initial concentration $M_0\delta(x_0,0)$ at position x_0 is [14]

$$M(x,t) = \frac{M_0}{2(\pi Dt)^{1/2}} \exp\left[\frac{-(x-x_0)^2}{4\,D\,t}\right] \tag{2}$$

where t is the time since the interaction.

In general, at depths greater than $\sim$1.7 mm, the lateral electric field is strong enough to compress the charge cloud and guide it to an anode (see Fig. 3). Therefore, we ignore diffusion once the charge drifts to depths greater than 1.7 mm. If $t_{1.7}$ is the time elapsed between the interaction time and the time that the cloud reaches a depth of 1.7 mm, then the concentration at this depth as a function of position can be obtained by substituting $t_{1.7}$ in place of t in Eq. (2). This time can be obtained using our electric field calculations as follows:

$$t_{1.7} = \frac{(0.17 - \mathrm{DOI})}{\mu E} \tag{3}$$

where DOI is the depth of interaction in cm, and E is the electric field component perpendicular to the detector surface. This field is constant to 1% between the top of the detector and 1.7 mm, and has a value of $\sim$930 V/cm. Since $t_{1.7}$ decreases with depth of interaction, the size of the cloud decreases as depth of interaction increases (Fig. 4).

5. Measurements

We studied the detector's response using collimated gamma-rays from a ^{57}Co radioactive source whose dominant emission is at 122 keV, with two weaker lines at 136 and 14.4 keV. The collimator uses a stack of precision, laser machined tantalum disks with holes ranging from 30 to 60 μm to form a 3 mm thick layer with a fine hole passing through it [2]. The hole is tapered to give a uniform intensity in its 30 μm aperture. This was placed $\sim$0.5 mm from the detector, and the radioactive source was $\sim$10 cm from the aperture. The position of the collimator was controlled by an X–Y stage with 10 μm precision.

Two adjacent anodes, the steering electrode and a cathode were coupled to Amptek A250 charge sensitive preamplifiers whose signals were processed by shaping, amplifying and triggering circuits, and digitized by ADCs to give the total

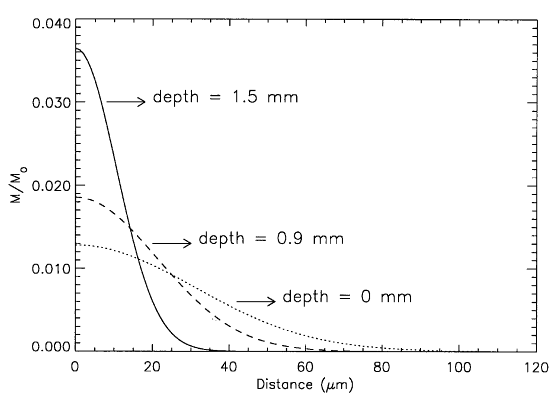

Fig. 4. Concentration of particles as a function of position for different interaction depths. Profiles show the concentration when the electrons have drifted to a depth of 1.7 mm. M_0 is the initial concentration.

signal on each electrode. An on-line program processed the data and built multiple spectra according to various event selection criteria [5,15]. If the signal on any electrode exceeded its threshold, the system was triggered and all pulse heights were measured and recorded to build event lists for off-line analysis.

We scanned perpendicular to the anode strips with the 30 μm collimator. The position with an equal number of counts at each anode was assumed to correspond to the center of the steering electrode. (see Section 6.2 for a discussion of this assumption.) Other positions were measured with respect to this point. The illumination point was centered on a cathode strip. Since anodes and cathodes are orthogonal, scanning the collimator across the anodes kept it centered on the cathode.

Interpretation of the measurements requires knowledge of the distribution of electron clouds for a given collimator position. This was determined in two steps. First, we calculated the flux of photons from the collimator to obtain the lateral distribution of interaction positions. Then, we convolved this distribution with the photoelectron path distribution. Fig. 5 shows the distribution of end points of photoelectron tracks along with the distribution of initial positions of interactions.

Since 122 keV gamma-rays have a range of ~1.5 mm, they interact throughout the detector, allowing us to study the dependence of charge sharing on depth. Because of hole trapping, the cathode signal decreases as depth of interaction increases, and the ratio of cathode signals to anode signals indicates the interaction depth [1,7]. We sorted events into depth ranges according to their cathode to anode ratios. Then, using the number of counts in each bin and the photoelectric absorption coefficient of CdZnTe for 122 keV photons, we calculated the boundaries of the depth ranges.

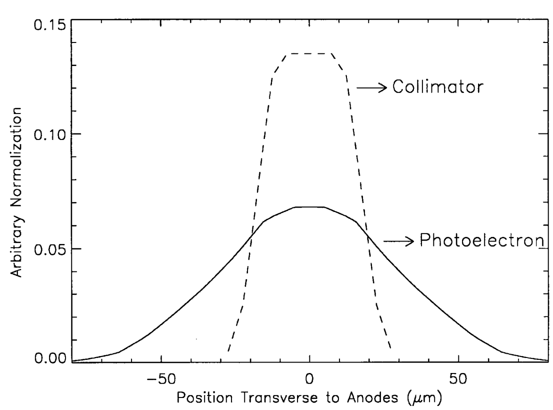

Fig. 5. The dashed line (collimator) shows the lateral distribution of interaction positions with respect to collimator position. The solid line (photoelectron) corresponds to the lateral distribution of endpoints of photoelectron tracks.

6. Results and interpretations

6.1. Charge sharing

For 122 keV events, the relative signals on the two neighbor anodes were found to be a strong function of beam position, as shown in Fig. 6. Well away from the steering electrode, at +250 μm, there is negligible charge sharing. All 122 keV (channel ~100) and 136 keV (channel ~113) interactions are collected at anode 2. The remaining continuum is background, except at channel ~12 (14.4 keV) where another line of ^{57}Co falls.

The position +250 μm plot in Fig. 6 is representative of the results from all positions greater than 100 μm, where charge sharing occurs for less than 1% of all interactions. For collimator positions less than 100 μm from the steering electrode, some events fall on a diagonal line representing full energy in the summed anode signals ($x + y = 122$ keV). At position 0 μm, three such lines are apparent, which correspond to 136, 122 and ~97 keV (escape peak). Negative positions mean the collimator is near anode 1, so most charge is collected by it, as indicated in the − 20 and − 100 μm panels. Since the points lie on a diagonal line, little charge is lost to the steering electrode the gap.

At 100 μm, there is a cluster of points circled in Fig. 6 which deposit ~25 keV (channel 20) in the neighbor anode. Since the K X-ray has an energy of ~25 keV and has a mean free path of 85 μm, we interpret these points as events whose K X-rays have propagated beyond the center of the steering electrode so that they have been collected by the neighbor anode.

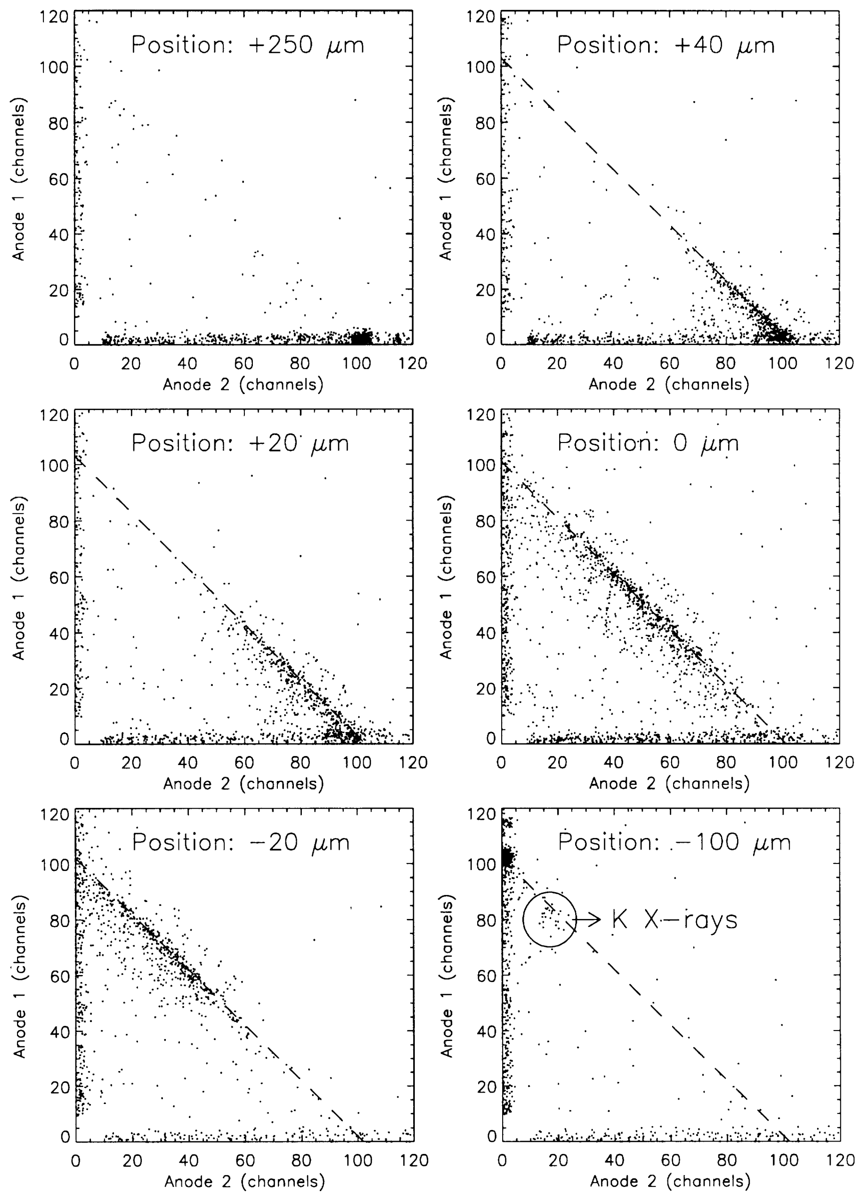

Fig. 6. Scatter plots of anode signals read out from the ADC. Each point represents one event. The positions represent the distance of the collimator from the center of the steering electrode (which is denoted by Position: 0 μm). The dashed lines represent the ideal case where sum of the charge collected by anodes 1 and 2 is proportional to the total charge deposited by 122 keV gamma-ray. 100 μm away from the steering electrode, K X-rays appear as a separate feature, see text for more details.

We examined the same data in more detail using spectra (Fig. 7) for the three collimator positions shown in Fig. 8. Position (A), at -250 μm, was directly above anode 1, and all of the charge was collected by anode 1. The energy resolution of the summed spectrum is 3% FWHM at 122 keV and the 14.4 keV line is resolved. Position (B) was 40 μm away from the center of the steering

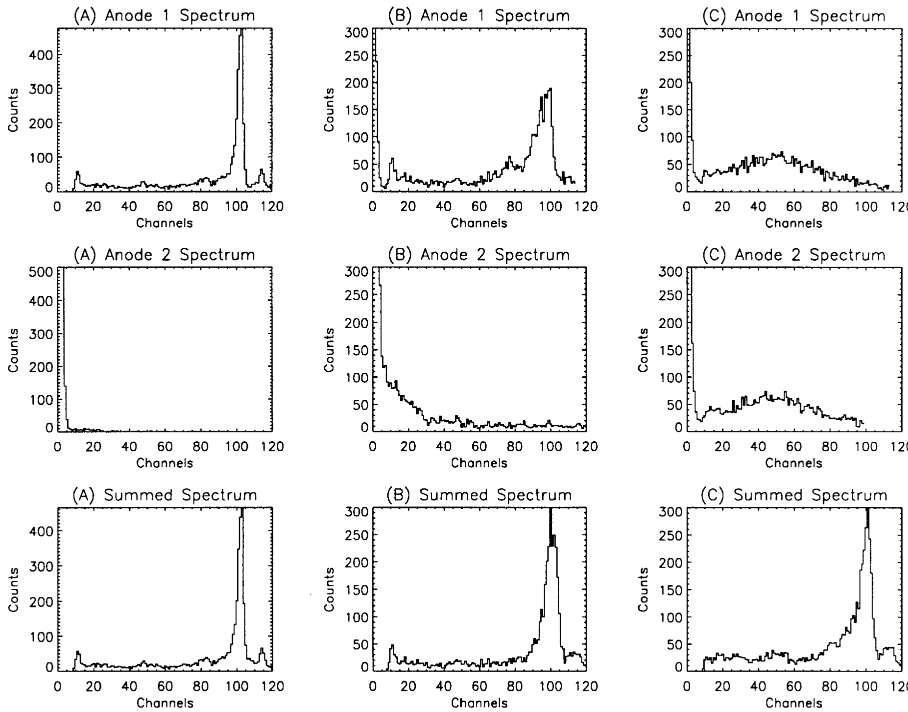

Fig. 7. Individual anode spectra and the summed anode spectra of ^{57}Co for the three different collimator positions (A–C) indicated in Fig. 8.c

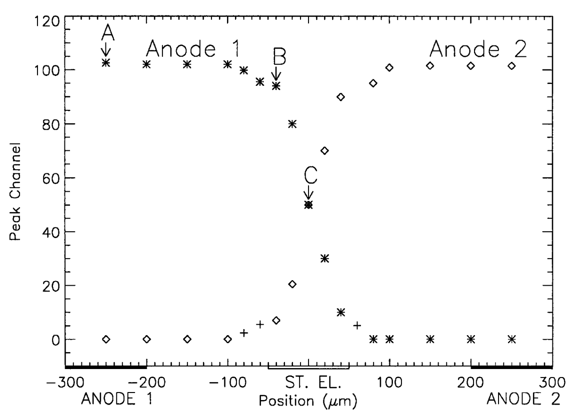

Fig. 8. Peak channels vs collimator positions for anodes 1 and 2. The inferred values (see text) are shown with "+" symbols.

electrode and charge sharing clearly affects the spectra. The anode 1 spectrum has a low energy tail along with an escape peak at channel ~ 80 while anode 2 has significant counts below channel 30 (36 keV). Compared to anode 1, the summed spectrum has a narrower peak and a less low energy tail. Position (C) was above the center of the steering electrode, and the two anodes have the same spectra, with peaks at channel ~ 50 (61 keV). In (C) all events shared charge, but a good spectrum was recovered by summing anode signals.

Positions (B) and (C)'s summed spectra have broader peaks than that for Position (A). This is due to three effects. First, adding signals means adding the electronic noise in quadrature. Second, we only summed anodes when the neighbor signal was larger than the noise level (4 channels). Therefore, if charge sharing occurred so that the signal on one anode was below the detection threshold of the electronics, it was not summed, producing an artificial low energy tail. However, this happens only at a very specific distance from the steering electrode and possibly affected summed spectrum in position (B). Third, and most important, was incomplete charge collection due to collection of electrons by the steering electrode and the gap. This will be discussed in detail in Section 6.3.

Spectral peaks were measured for both anodes at 17 beam positions and the results are plotted in Fig. 8. At three positions, the smaller peaks were too close to the noise to be determined. For these cases an "inferred peak", equal to channel 102 minus the larger peak, is plotted. There is a smooth transition in peak channel from channel 102 (full signal) to zero signal over a $\pm 80\ \mu m$ region around the steering electrode. Note that this result is the convolution of the intrinsic transition with the collimator response of $\sim \pm 20\ \mu m$ (dashed line in Fig. 5). Thus, the intrinsic transition occurs in $\sim \pm 60\ \mu m$.

6.2. Effects of diffusion and photoelectron range

We expect charge sharing to be greater for interactions near the cathode, since the cloud must drift through a greater depth, diffusing more. We showed this to be the case by comparing the sharing effects at the top and the bottom of the detector for a collimator position 40 μm away from the center of the steering electrode, as shown in Fig. 9. Panel (a) is for interactions in the top 0.2 mm of the detector and significant charge sharing occurs. However, most of the interactions at the bottom of the detector are fully collected at anode 1, as shown in panel (b).

Quantitative studies of diffusion were made by comparing the onset of sharing versus beam position with the predicted onset. This was calculated from the photoelectron range distribution (Fig. 5) modified by the predicted broadening due to diffusion (Eq. (2) and Fig. 4). This produced a predicted charge distribution as a function of distance from the collimator and depth of interaction. We defined the onset of charge sharing for each depth as the collimator position at which the neighbor anode received more than 5% of the signal for at least 5% of all the events. For 5% of all interactions, the photoelectron range is greater than 45 μm, as determined by integrating the solid curve in Fig. 5. By using Eqs. (2) and (3), we predicted the distance beyond which 5% of the electrons reside when the electron cloud reaches at a depth of 1.7 mm, and called it $L(5\%)$. Then the sharing onset is expected to occur at $45\ \mu m + L(5\%)$. This distance was calculated for three depths and compared with measurements, with the results shown in Table 1.

Average depths, depth ranges, $L(5\%)$ values, and predicted onsets are shown in the first four columns of Table 1. In the last two columns are the collimator positions where the onsets were observed and the nearest position where no sharing is observed. The results show that observational onsets are within the uncertainties of the estimated onsets.

Uncertainties in the observations correspond to the positioning of the collimator, and uncertainties

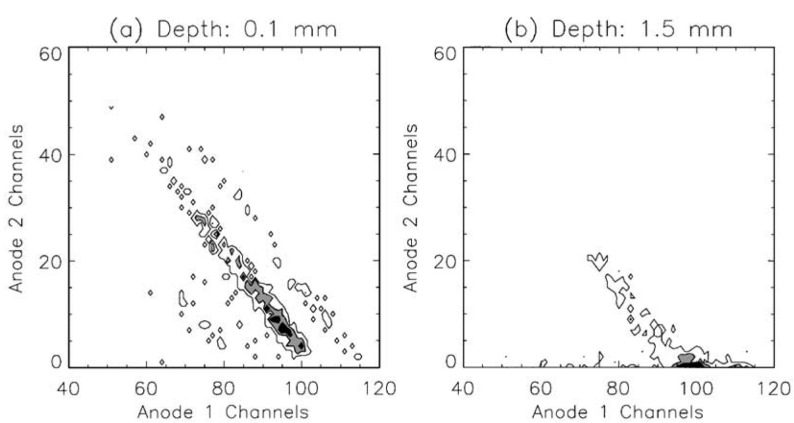

Fig. 9. The depth dependence of charge sharing. Figures are contour plots of 2D histograms of anode 1 vs anode 2 signals. Darker regions indicate higher density of points. The collimator is at $-40\ \mu m$. Panels (a) and (b) correspond to average depths of 0.1 and 1.5 mm, respectively.

Table 1
Predicted and observed onset of charge sharing

Avg. depth (mm)	Depth range (mm)	$L(5\%)$ (μm)	Predicted (μm)	Observed (μm)	No sharing (μm)
0.1	0–0.2	50^{+1}_{-0}	95^{+1}_{-10}	95 ± 5	105 ± 5
0.44	0.35–0.53	43^{+2}_{-0}	88^{+2}_{-10}	80 ± 5	100 ± 5
1.1	0.9–1.3	30^{+4}_{-0}	75^{+4}_{-10}	65 ± 5	85 ± 5

in the calculations were combinations of various effects such as sampling preferentially lower depths within one depth range, uncertainty of charge sharing due to K X-ray interactions, and the assumption that the initial concentration of the electron cloud is a delta function. We also assumed that the point where charge is shared equally is the center of the steering electrode. We did not have an experimental measurement to verify this assumption; however, we observed that the charge is shared equally at each depth range for this collimator position. Even if this position does not correspond to the center of the steering electrode it still defines the plane beyond which the charges are collected by the neighbor anode. Since the collimator positions are measured with respect to this plane, this assumption does not introduce uncertainties in our results. We also estimated the contribution of holes to the charge sharing phenomenon using our simulations described in Kalemci et al. [1]. We used a hole mobility of 40 cm^2/V s and a hole trapping time of 650 ns in our simulations. The results showed that at the depth range the sharing onsets were calculated, 0.1–1.3 mm, the holes contribute less than 1% to the neighbor anode signals and is neglected.

6.3. Charge loss to the steering electrode and gaps

As noted earlier, for interactions within ~ 60 μm of the steering electrode, the summed anode signal is reduced by a few percent and shows tailing. A simulation neglecting diffusion predicts that electrons from these events would drift only to the steering electrodes, producing no signal on the anodes. We showed in Kalemci et al. [1] that, for some of the interactions, the steering electrode has positive signals, which means that it collects electrons for some events. However, if the number of field lines ending at the steering electrode is smaller than predicted by the model and/or the electron cloud is larger than ~ 100 μm, only a small fraction of the electrons will be collected by it. This could explain the lack of full energy signals on the steering electrode.

It is difficult to interpret the steering electrode pulses to study such effects. Since steering electrodes are joined together their weighting potentials extends throughout the detector. (See Kalemci et al. [1] for weighting potential calculations.) They are sensitive to both electron and hole transport at all depths of interaction and one cannot extract the signal solely due to electrons reaching the steering electrode. Therefore, to look for a charge loss to the steering electrode or the gaps, we analyzed summed anode spectra, since anode signals are not as depth dependent as steering electrode signals due to the small pixel effect.

We compared the summed anode spectrum for a collimator position above anode 2 with that of above the steering electrode. This analysis was done for various depth ranges, and the results are shown in Fig. 10. At each depth, we considered the shift of line centroid over the steering electrode relative to that over the anode. Near the top of the detector (0.1 mm), the shift is $\sim 1\%$. For deeper interactions, the shift became larger. For the average depth of 1.5 mm, the centroid shifted $\sim 9\%$. The increase of centroid shift with increasing depth is consistent with the diffusion of electron cloud with time, because, for deeper interactions, the electrons have less time to diffuse and the charge cloud is smaller. Therefore, the steering electrode collects more of the electrons.

These data allow us to estimate the size of the detector region where the field lines end at the steering electrode. This is equal to the lateral extent of the part of the charge cloud which drifts

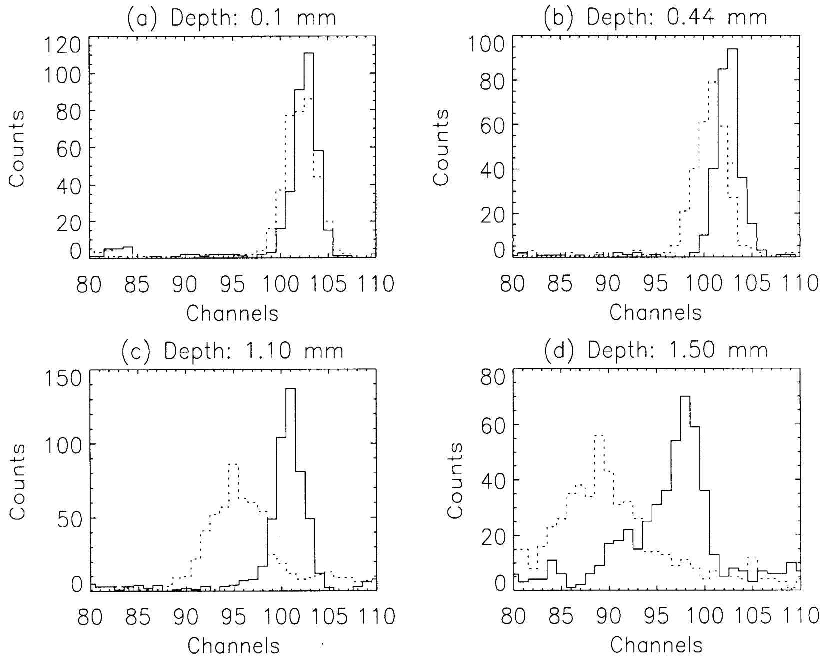

Fig. 10. Depth dependence of signal lost to the steering electrode. Each panel contains two spectra, one for collimator directly above one anode (solid line) and other directly above the steering electrode. These show that, as the interactions get deeper, the steering electrode collects more charge, reducing the summed anode signal.

to the steering electrode. At the depth range, 1.1–1.7 mm, the maximum charge lost is $\sim 15\%$ (Fig. 10d). Assuming these events occurred at 1.7 mm, and the photoelectrons moved towards the steering electrode with no additional broadening, a diffusion time of $t = 40$ ns results in 15% of the electrons being within ± 2 μm of the charge cloud's center. Thus, the region with field lines ending on the steering electrode measures just ± 2 μm. However, our electric field calculation (Fig. 3) predicted a ± 20 μm region. This would result in the majority of electrons being collected by the steering electrode for interactions above it at any depth. We therefore conclude that the model overestimates the number of field lines ending at the steering electrode.

7. Conclusion

We have investigated charge collection by various electrodes and charge sharing between two anodes of a 2 mm thick CZT strip detector with 500 μm pitch electrodes. A 30 μm collimated beam of 122 keV gamma-rays was used to study the detector response at various positions and the cathode signal was used to infer depth of interaction. The results were interpreted in the context of our charge collection model.

We found that diffusion is a very important mechanism causing charge sharing. For an interaction with minimal depth in the detector, the electron cloud size increases to ~ 100 μm due to diffusion while it drifts 2 mm to the anodes in a ~ 1000 V/cm field. Charge sharing occurs over 24% of our detector volume for our specific electrode pattern.

The solution of Fick's equation predicts that the size of the cloud changes as a function of depth. We tested this by mapping the onset of charge sharing as a function of interaction depth. The results were in good agreement with the calculated onsets. Another important mechanism affecting charge sharing is the photoelectron range. Without considering its effects, the predicted onsets in Table 1 would be reduced by $\sim 20\ \mu m$, contrary to the observed onsets.

Our detector model predicts that interactions above the steering electrode would have the majority of their electrons collected by the steering electrode, but the laboratory tests indicate that this is not the case. Rather, $> 90\%$ of the electrons reach the anodes for interactions only 0.5 mm above the steering electrode. This implies that the simulation overestimates the number of field lines ending at the steering electrode. A similar effect was reported in a study by Prettyman et al. [9] where they discussed possible causes, such as band bending near the anodes, surface effects, and microscopic defects.

In the region where charge sharing occurred, the summed anode signal was at 91–99% of that for single anode events. The deficit represents electrons lost to the steering electrode and the gaps. It appears to be possible to correct for these effects. First, the ratio of cathode-to-anode signals can be used to infer the depth, allowing a depth dependent correction to the energy for hole trapping as shown by Kalemci et al. [1]. Second, for shared events, the ratio of the signals on the two anodes indicates the transverse position which can be used, along with the depth, to correct for the signal lost to the steering electrode and the gaps. Such a full correction is the subject of future work.

Acknowledgements

This work was supported by NASA SR&T Grant NAG5-5111 and NASA Grant NAG5-8498. Technical support was provided at UCSD by Fred Duttweiler, George Huszar, Charles James, Phillippe Leblanc, David Malmberg, Ron Quillan and Ed Stephan. Authors would like to thank Richard Rothschild, William Heindl, John Tomsick and R.T. Skelton for their valuable discussions. We also would like to thank Kimberly Slavis at WU for her contributions. Emrah Kalemci was partially supported by TUBITAK.

References

[1] E. Kalemci et al., SPIE Proceedings, Denver, Vol. 3768, July 19–23, 1999, p. 360.
[2] J.L. Matteson et al., SPIE Proceedings, Denver, Vol. 2859, August 7–8, 1996, p. 58.
[3] H.H. Barret, et al., Phys. Rev. Lett. 75 (1995) 156.
[4] P.N. Luke, Proceedings of the Ninth International Workshop on Room Temperature Semiconductor X- and Gamma Ray Detectors, Associated Electronic and Applications, Grenoble, France, 1995.
[5] J.L. Matteson et al., SPIE Proceedings, San Diego, Vol. 3445, July 22–24, 1998, p. 445.
[6] Y.F. Du, et al., IEEE Trans. Nucl. Sci. NS-46 (1999) 844.
[7] Z. He, et al., Nucl. Instr. and Meth. A 439 (2000) 619.
[8] A.E. Bolotnikov, et al., Nucl. Instr. and Meth. A 432 (1999) 326.
[9] T.H. Prettyman et al., SPIE Proceedings, Denver, Vol. 3768, July 19–23, 1999, p. 27.
[10] M.L. Cherry et al., SPIE Proceedings, Denver, Vol. 3765, July 19–23, 1999, p. 539.
[11] S. Ramo, Proc. I. R. E. 27 (1939) 584.
[12] Maxwell 2D Field Simulator, Ansoft Corporation, Four Station Square, Suite 200, Pittsburgh, PA 15219-1119, www.Ansoft.com.
[13] NIST, Physical Reference Data, ESTAR, http://physics.nist.gov/PhysRefData/Star/Text/ESTAR.html.
[14] W.R. Beam, Electronics of Solids, Mc-Graw Hill, New York, 1965, p. 282.
[15] K.R. Slavis, SPIE Proceedings, San Diego, Vol. 3445, July 22–24 1998, p. 169.